Flexible MIL-53(Al)/Biochar Composite for Enhanced Norfloxacin Removal: Synergistic Effects and Adsorption Mechanisms

Pisit Phayutcharoenkun[1], Samson B. Akindoye[1], Rajendran Chandran[1], Anh N. Phan[2], Long T. Duong[3], Amornchai Arpornwichanop[1,4] and Phuet Prasertcharoensuk[1,4*]

[1] Department of Chemical Engineering, Faculty of Engineering, Chulalongkorn University, Bangkok 10330, Thailand

[2] School of Engineering, Chemical Engineering, Newcastle University, Newcastle Upon Tyne NE1 7RU, United Kingdom

[3] School of Engineering, Lancaster University, Lancaster LA1 4YW, United Kingdom

[4] Center of Excellence in Process and Energy Systems Engineering, Department of Chemical Engineering, Faculty of Engineering, Chulalongkorn University, Bangkok, 10330, Thailand

*Corresponding authors: phuet.p@chula.ac.th

Abstract

The presence of antibiotic contaminants, particularly norfloxacin (NRFX) in aquatic environments poses a significant threat to ecosystems and public health, due to their persistence, bioaccumulation, and contribution to antimicrobial resistance. In this study, a novel MIL-53(Al)/biochar composite was synthesized and applied for NRFX removal from wastewater. The synthesized composite exhibited a high surface area (806 m^2/g) and mesopore structure, promoting to improved dispersion and adsorption efficiency. Under optimal conditions (20 mg/L NRFX, 40 mg/L adsorbent, 30 °C, 120 min), the composite achieved a maximum adsorption capacity of 357 mg/g, surpassing most reported antibiotic sorbents (< 250 mg/g). The superior performance was attributed to the synergistic integration of MIL-53(Al) flexible "wine-rack" framework with the oxygen-functionalized, mesoporous carbon matrix of bamboo-derived biochar, facilitating multiple adsorption mechanisms, including electrostatic attraction, hydrogen bonding, π–π interactions, and pore-filling effects. These findings highlight the potential of MIL-53(Al)/BC as a cost-effective, sustainable, and high-performance adsorbent with strong potential for real-world remediation of antibiotic-contaminated wastewater under diverse environmental conditions.

Keywords: Norfloxacin, MIL-53(Al), Biochar, Adsorption, Wastewater treatment.

1. Introduction

The presence of emerging pollutants in aquatic environments, particularly pharmaceuticals and personal care products (PPCPs), has increased concerns due to their persistence, bioaccumulation, and adverse ecological impacts [1-3]. Municipal and hospital wastewater streams frequently contain antibiotics such as tetracycline, amoxicillin, ciprofloxacin, ampicillin, and norfloxacin (NRFX) [4-6]. Due to incomplete metabolism in humans and animals, these antibiotics are often excreted in active forms, leading to their continuous release into natural water bodies [7-8]. This persistence contributes significantly to environmental contamination and plays a critical role in the development of antimicrobial resistance (AMR), a major global public health challenge [9-11]. NRFX, a broad-spectrum fluoroquinolone antibiotic, is widely prescribed in both human and veterinary medicine for its therapeutic efficacy and low toxicity [12-14]. Furthermore, its high aqueous solubility and chemical stability render it recalcitrant to traditional biological and physical wastewater treatment processes [15]. Reported environmental concentrations range from < 0.1 to >10 μg/L in surface waters and up to 100 μg/L in untreated hospital effluents [16, 17]. Even at trace levels e.g. ≤ 1 μg/L, NRFX can disrupt aquatic ecosystems and accelerate the proliferation of antibiotic-resistant microbial strains [9, 11, 17]. These concerns have driven the search for advanced treatment technologies capable of selectively and efficiently removing such contaminants from water. Various approaches including microbial degradation, advanced oxidation processes, adsorption, membrane filtration, and photodegradation have been explored [18, 19]. Among these, adsorption has emerged as a particularly attractive method due to its operational simplicity, cost-effectiveness, high efficiency, and scalability, especially when high-surface-area porous adsorbents are employed [20]. Porous materials such as activated carbon, zeolites, and graphene-based structures have demonstrated potential for pharmaceutical pollutants removal [20-22]. However, the current adsorbents still encounter several challenges such as low adsorption capacity (< 250 mg/g), low selectivity (60-75%), high regeneration costs, and performance losses in the presence of competing ions [23, 24]. Therefore, the development of next-generation adsorbents with high adsorption capacity, selectivity and sustainability is urgently needed.

Metal–organic frameworks (MOFs), particularly aluminum terephthalate MIL-53(Al), have gained attention for environmental remediation owing to their high surface area, tunable pore structure, and excellent chemical and thermal stability [25, 26]. The distinctive “wine-rack” architecture of MIL-53(Al) provides structural flexibility, enabling its pores to reversibly expand or contract in response to target pollutants. This dynamic behavior increases the accessibility of active

sites and facilitates the adsorption of bulky organic molecules such as NRFX, thereby improving overall adsorption performance. In contrast, conventional MOFs with rigid frameworks (e.g. MIL-101, UiO-66, and ZIF-8) exhibit fixed pore structures that restrict their adaptability toward large molecular species [27]. Moreover, their large-scale application of pristine MOFs remains constrained by high synthesis costs, limited water stability, and challenges in recovery and reuse [28]. To overcome these limitations, the integration of MOFs with biochar has emerged as a promising approach that combines the structural tunability and adsorption affinity of MOFs with the sustainability, hierarchical porosity, and rich surface chemistry of biochar. The incorporation of biochar not only enhances the mechanical and chemical stability of MOFs but also increases overall adsorption efficiency by introducing additional mesoporous channels and oxygen-containing functional groups. Biochar, an eco-friendly carbon-rich material derived from biomass pyrolysis, offers low-cost production, high porosity, abundant surface functionalities, and excellent environmental compatibility [29]. This hybridization approach therefore provides a synergistic pathway to improve adsorption performance while promoting material sustainability. However, despite numerous studies on MOF–biochar hybrids for antibiotic removal, no reported material has yet demonstrated a NRFX adsorption capacity exceeding 250 mg/g [30-35], indicating that the interfacial synergy between MOF and biochar components remains under optimized.

In this study, a novel composite material comprising MIL-53(Al) and bamboo-derived biochar (MIL-53(Al)/Biochar) was synthesized and characterized for NRFX removal. This hybrid integrates the flexible framework of MIL-53(Al) with the oxygen-functionalized, mesoporous carbon matrix of biochar to achieve high adsorption capacity, rapid uptake kinetics, and enhanced structural stability. The primary objectives of this work are: (i) to synthesize and comprehensively characterize the MIL-53(Al)/biochar hybrid; (ii) to investigate the effects of key operating parameters including temperature, adsorbent dosage and NRFX concentration and contact time on adsorption performance, and (iii) to elucidate the underlying NRFX adsorption mechanisms through batch adsorption experiments. Overall, this study provides new insights into the rational design of sustainable, high-performance MOF–biochar composites for the efficient removal of antibiotic-contaminated from wastewater.

2. Materials and methods

2.1 Materials

Commercial-grade bamboo-derived biochar was supplied by Thai Carbon & Graphite Co., Ltd. (Thailand) and used as the carbon precursor. Aluminum nitrate nonahydrate ($Al(NO_3)_3 \cdot 9H_2O$, 99%), benzene-1,4-dicarboxylic acid (BDC, 99%), N,N-dimethylformamide (DMF, 99.8%), hydrochloric acid (HCl, 37%), sodium hydroxide (NaOH, ≥ 98%), potassium hydroxide (KOH, ≥ 85%), and acetone (≥ 99.9%) were purchased from Sigma–Aldrich. All solutions were prepared with deionized water.

2.2 Preparation methods

2.2.1 Activation of Bamboo derived biochar

Commercial-grade bamboo-derived biochar supplied by Thai Carbon & Graphite Co., Ltd., Thailand was used as the carbon precursor. To enhance its surface area and porosity of the biochar, the biochar was chemically activated following a procedure reported in literature [36] (Figure 1). The biochar was impregnated with KOH at a mass ratio of 1:2 (biochar:KOH) and then calcined in a horizontal tube furnace under N_2 atmosphere (20 dm^3/h). The temperature was ramped at 5 °C/min to 600 °C and held for 2 h. After cooling to room temperature, the activated biochar was washed repeatedly with deionized water and subsequently treated with either 0.1 M HCl or 0.1 M NaOH until neutral pH, then dried at 100 °C for 24 h and stored in a desiccator.

2.2.2 Synthesis of MIL-53(Al)

MIL-53(Al) was synthesized via a solvothermal method adapted from the literature [37] as shown in Figure 1. Aluminum nitrate nonahydrate ($Al(NO_3)_3 \cdot 9H_2O$, 1.915 g, 5 mmol), and benzene-1,4-dicarboxylic acid (BDC, 0.415 g, 2.5 mmol) were dissolved in 20 mL of distilled water and 10 mL of N,N-dimethylformamide (DMF) stirring until a clear solution was obtained. The mixture was transferred to 50 mL Teflon-lined stainless-steel autoclave and heated at 150 °C for 24 h. After natural cooling to room temperature, the white precipitate was collected by vacuum filtration and washed several times with deionized water and oven-dried at 150 °C overnight. To remove residual solvent and unreacted linkers, the dried powder was soaked in acetone for 7 days (fresh solvent every 24 h), then filtered through a 50 µm nylon mesh and dried at 120 °C before use. The use of fresh solvent in each washing cycle ensured complete removal of unreacted precursors and byproducts, thereby enhancing the purity of the synthesized material.

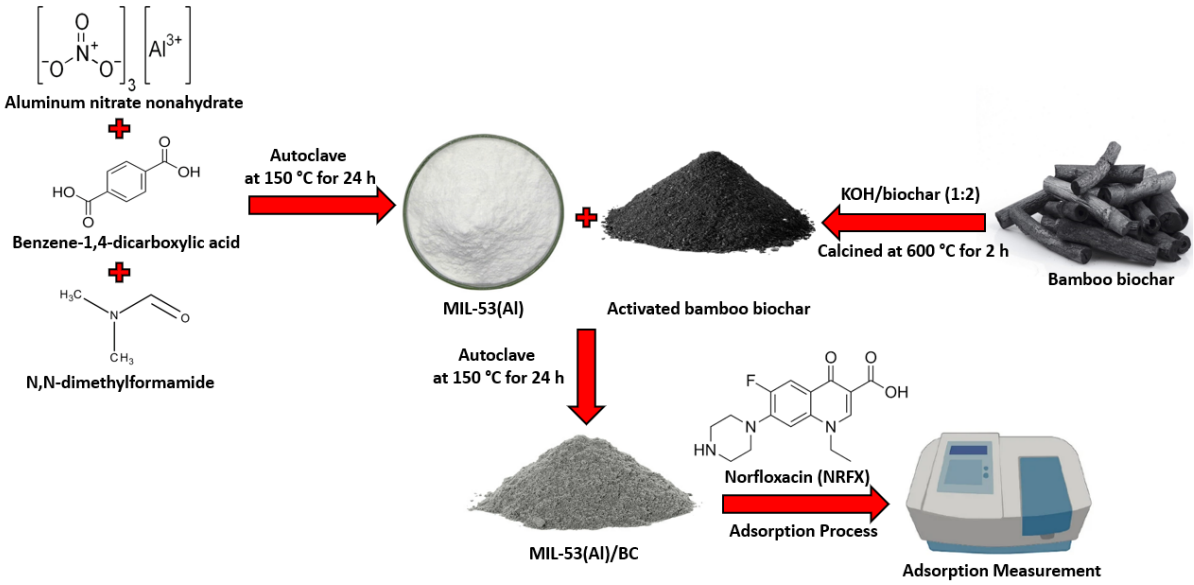

Figure 1: The synthesis pathways of MIL-53(Al) and MIL-53(Al)/biochar composite for NRFX adsorption.

2.2.3 Synthesis of MIL-53(Al)/Biochar Composite

MIL-53(Al)/BC was synthesized by in situ solvothermal growth of MIL-53(Al) on activated biochar (Figure 1). Aluminum nitrate nonahydrate ($Al(NO_3)_3 \cdot 9H_2O$, 1.915 g, 5 mmol) and benzene-1,4-dicarboxylic acid (BDC, 0.415 g, 2.5 mmol) were dissolved in 20 mL of distilled water and 10 mL of N,N-dimethylformamide (DMF) with stirring until a clear solution formed. Activated biochar (0.4 g) was added into the precursor solution and sonicated for 15 min, followed by magnetically stirring for 30 min to ensure homogeneous suspension. The mixture was transferred to a 50 mL Teflon-lined stainless-steel autoclave and heated at 150 °C for 24 h. After cooling to room temperature, the grey solid was collected by filtration through a 50 µm nylon membrane, washed three times with deionized water, and oven dried at 150 °C for 24 h and stored in a desiccator until use.

2.3 Characterization

Fourier-transform infrared spectroscopy (FT-IR) was carried out to characterize the functional groups in absorbent material using a ReactIRTM 4000 FT-IR spectrometer, with a scan range from 400–4000 cm^{-1} with a resolution of 4 cm^{-1}. The physical morphology and elemental distribution of the absorbent material were examined by a Hitachi TM 3030 Scanning Electron Microscope (SEM) equipped with an Energy Dispersive X-ray detector (EDX), operated at a 15 kV accelerating voltage. The crystalline components of the absorbent were analyzed by Power X-ray diffraction (PXRD) using Panalytical X'Pert Pro multipurpose diffractometer (MPD) equipped with an X'Celerator and a

secondary monochromator (Cu-Kα radiation), operated at 40 kV, 40 mA and wavelength ($K_{\alpha 1}$) of 0.15 nm. The scanning was performed over a 2θ range of 5–55° with a step size of 0.03°. Thermogravimetric analysis (TGA) of the absorbent was undertaken using a Perkin Elmer STA 6000 to assess thermal degradation, solvent removal, and decomposition profile solid residues of absorbent material by measurement of weight loss as a function of temperature and time under a controlled atmosphere (N_2). The specific surface area of absorbent material was determined by the Brunauer Emmett Teller (BET) nitrogen physisorption isotherms conducted at 77 K using a Thermo Scientific Surfer Gas Adsorption Porosimeter. Nitrogen adsorption–desorption isotherms were collected, and the volume of N_2 adsorbed was recorded and processed using Surfer software.

2.4 Adsorption experiments

Batch adsorption experiments were performed in a temperature-controlled orbital shaker at 50 rpm to evaluate the NRFX removal efficiency of the synthesized adsorbents and all experiments were triplicated. The synergistic effect of key operating parameters including adsorbent dosage (40-80 mg/L), initial NRFX concentration (10–50 mg/L), contact time (15–120 min), and temperature (30-70 °C) on adsorption performance were investigated. After equilibration, the adsorbents were separated by filtration, and the supernatants were analyzed using a UV-Vis spectrophotometer (Shimadzu UV-2600). The adsorbed amount of NRFX onto the adsorbent (q_e, mg/g) was calculated using the following equation:

$$q_e = \frac{(C_0 - C_e) \times V}{m}$$

where C_0 is initial concentration of NRFX (mg/L); C_e is equilibrium concentration of NRFX (mg/L); V is volume of the solution (L), and m is mass of the adsorbent (g)

3. Results and discussion

3.1 Physicochemical Characterization of the Adsorbents

3.1.1. Powder X-Ray Diffraction (PXRD) analysis

PXRD confirmed the phase purity of all synthesized materials (Figure 2). Bamboo biochar (Figure 2c) shows a broad halo at ~24°, characteristic of the amorphous carbon structure derived from lignocellulosic pyrolysis. The synthesized MIL-53(Al) (Figure 2b) exhibits intense reflections at

8.7°, 10.0°, 12.8°, 17.7° and 22.4° 2θ, which identical to those of the MIL-53(Al) commercial reference those reported in literature [38, 39] confirming the successful formation of high-purity MIL-53(Al). The MIL-53(Al)/biochar composite (Figure 2a) retained all characteristic MIL-53(Al) reflections without additional peaks attributable to Al_2O_3, $Al(OH)_3$, or graphitic carbon, indicating that the MIL-53 lattice structure remained intact upon immobilization on biochar. The slight attenuation and broadening of peaks may be attributed to: (i) oxygen-rich functional groups on the biochar surface, (ii) partial X-ray shadowing by the amorphous carbon matrix, (iii) moderate crystallite-size reduction, (iv) preferred orientation during composite formation, and (v) restricted crystal growth on a heterogeneous substrate. The absence of impurity peaks confirms that biochar incorporation preserves the structural integrity of MIL-53(Al).

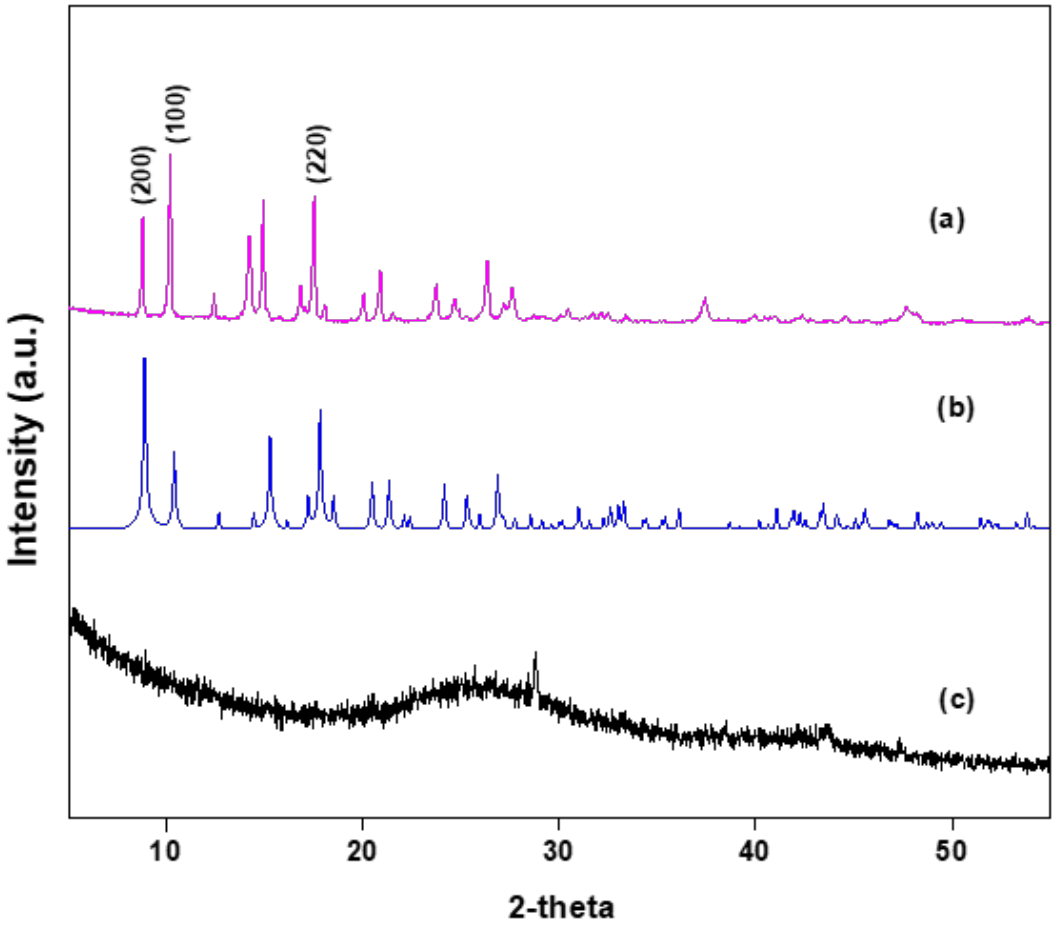

Figure 2: Powder X-ray Diffraction (PXRD) patterns of (a) MIL-53(Al)/biochar, (b) MIL-53(Al) and (c) activated bamboo biochar

3.1.2. Morphology and surface area of the synthesized absorbent

N_2 adsorption-desorption isotherms at 77 K are presented in Figure 3, and the corresponding textural parameters are summarized in Table 1, including the BET surface area and the t-plot micropore area and volume. As illustrated in Figure 3c, the activated bamboo biochar (BC) exhibits a mesoporous type IV isotherm with an H3 type hysteresis loop [40]. The BC sample presents BET surface area of 432.4 ± 8 m^2/g, a total pore volume of 0.3 cm^3/g, and the average pore diameter of 2.3 nm. The MIL-53(Al) shows a type IV isotherm with a pronounced H4 loop (Figure 3b) consistent with one-dimensional structure [41]; a BET surface area is 650.5 ± 12 m^2/g, with approximately 68 % of the porosity attributed to micropores and a dominant pore width centered at 2.2 nm. The MIL-53(Al)/BC composite successfully integrates the characteristics of both components, exhibiting a mixed H3/H4 hysteresis profile (Figure 3a), confirming the coexistence of mesopores from biochar and micropores from MIL-53(Al). This synergistic architecture markedly enhanced the composite's textural properties; its BET surface area (806.0 ± 11 m^2/g) and total pore volume (0.5 cm^3/g) are 24% and 66% higher, respectively, than those of the pure MIL-53(Al) (Table 1). Moreover, the surface area of the MIL-53(Al)/BC composite is considerably greater than that of conventional MOF materials, which typically range between 200 and 700 m^2/g e.g., MIL-101 (222 m^2/g), MIL-53(Fe) (240 m^2/g), UiO-66 (580 m^2/g), ZIF-8 (210 m^2/g), and MOF-5 (600 m^2/g) [27, 28,30-35]. This notable enhancement underscores the synergistic role of biochar incorporation in inhibiting MIL-53(Al) particle agglomeration, promoting uniform nanocrystal dispersion, and creating inter-crystalline mesoporous channels that substantially increase the number of accessible adsorption sites.

The increased surface area (from 650 m^2/g to 806 m^2/g) and enlarged pore size distribution (from 2.2 nm to 2.7 nm) are attributed to the heterogeneous nucleation of MIL-53(Al) nanocrystals on the biochar surface. The oxygen-rich biochar provides abundant anchoring sites that inhibit MOF crystallite aggregation and promote the formation of intercrystalline mesogaps, yielding a hierarchical micro–mesoporous architecture [42], which facilitates rapid intraparticle diffusion and contributes to the composite’s superior adsorption capacity toward norfloxacin. This formation of a hierarchical micro-mesoporous architecture is visually confirmed by morphological observations (Figure 4) where the rougher surface of MIL-53(Al)/BC (Figure 4a) contrasts with the smoother textures of MIL-53(Al) (Figure 4b) and activated bamboo biochar (Figure 4c).

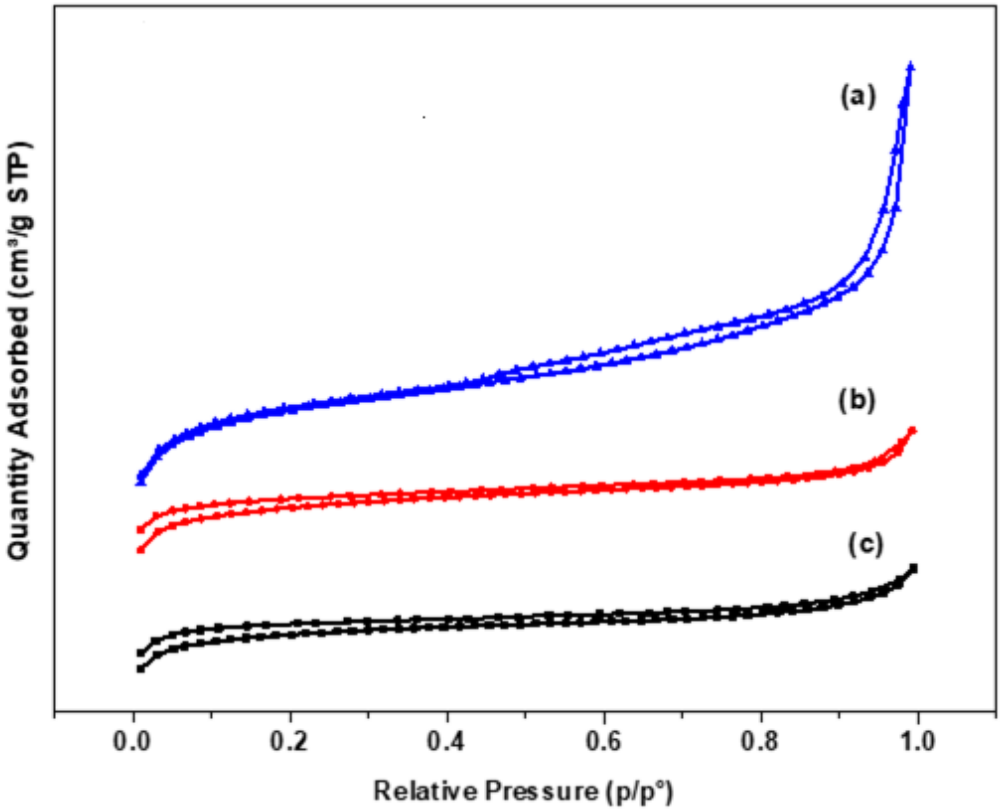

Figure 3: N_2 adsorption–desorption isotherms at 77 K of (a) MIL-53(Al)/biochar, (b) MIL-53(Al) and (c) activated bamboo biochar

Table 1: BET surface area, micropore and external surface areas (t-plot), total pore volume, and average pore diameter of MIL-53(Al), MIL-53(Al)/biochar composite and activated bamboo biochar derived from N_2 adsorption–desorption isotherms at 77 K

Sample No.	Material	Surface area (m^2/g)	t-Plot Micropore Area (m^2/g)	t-Plot External surface area (m^2/g)	Total Pore volume (cm^3/g)	Pore size (nm)
1	MIL-53(Al)/biochar	806.0	355.2	76.9	0.5	2.7
2	MIL-53(Al)	650.5	552.1	98.2	0.4	2.2
3	Activated bamboo biochar	432.4	618.9	187.4	0.3	2.3

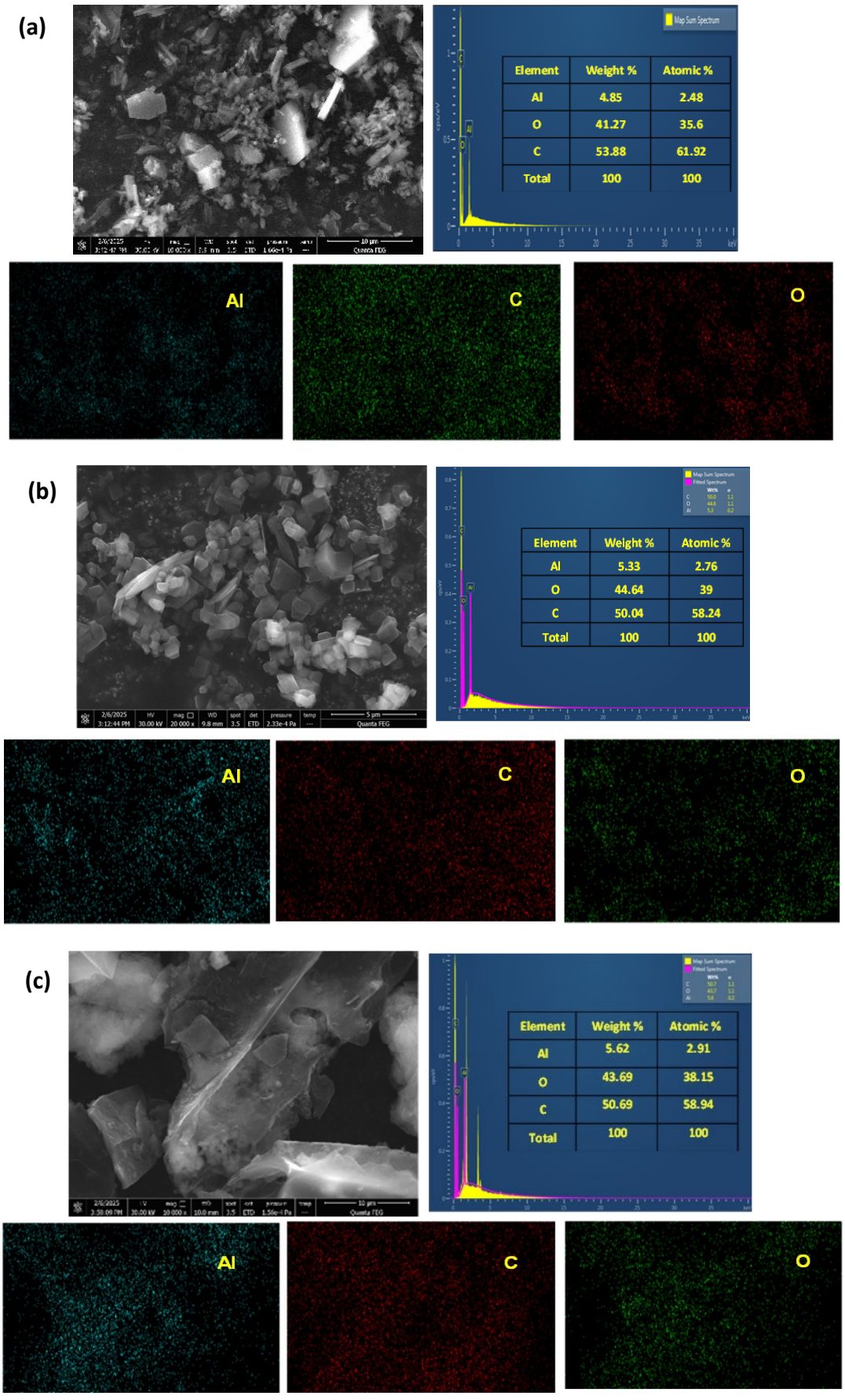

Figure 4: SEM images and EDXS mapping of (a) MIL-53(Al)/biochar, (b) MIL-53(Al) and (c) activated bamboo biochar

3.1.3 Fourier-Transform Infrared Spectroscopy (FT-IR) analysis

FT-IR spectroscopy (Figure 5) was used to identify functional groups contributing to NRFX adsorption. The pristine MIL-53(Al) exhibited characteristic vibrations of the 1,4-benzenedicarboxylate (BDC) linker, including $–COO^-$ stretches at 1608 and 1512 cm^{-1} and symmetric stretches at 1435 and 1417 cm^{-1} and a weal shoulder at 1669 cm^{-1} from uncoordinated –COOH groups [43]. The Al–OH bending mode of trans-corner-sharing $AlO_4(OH)_2$ was observed at 989 cm^{-1} [44]. Activated biochar shows a broad O–H stretching envelope (≈ 3294 cm^{-1}) from phenolic and alcoholic groups, an aliphatic C–C stretch at 3089 cm^{-1}, a C–O–C stretch at 1693 cm^{-1}, and aromatic C=C bending at 730 cm^{-1} [45]. In the MIL-53(Al)/BC composite, all major MIL-53(Al) and biochar bands were retained, confirming that the MOF's "wine-rack" framework survived solvothermal growth on biochar, in agreement with PXRD results (Figure 2). Broadening and red-shifting of the O–H stretch indicated new hydrogen-bonding interactions between biochar hydroxyls and MIL-53(Al) linkers or Al–OH sites [46, 47]. Thus, the coexistence of phenolic O–H, coordinatively unsaturated Al–OH, and extended aromatic domains creates complementary hydrogen-bond donor/acceptor sites and π–π stacking interfaces, rationalizing the composite's superior NRFX adsorption performance [48].

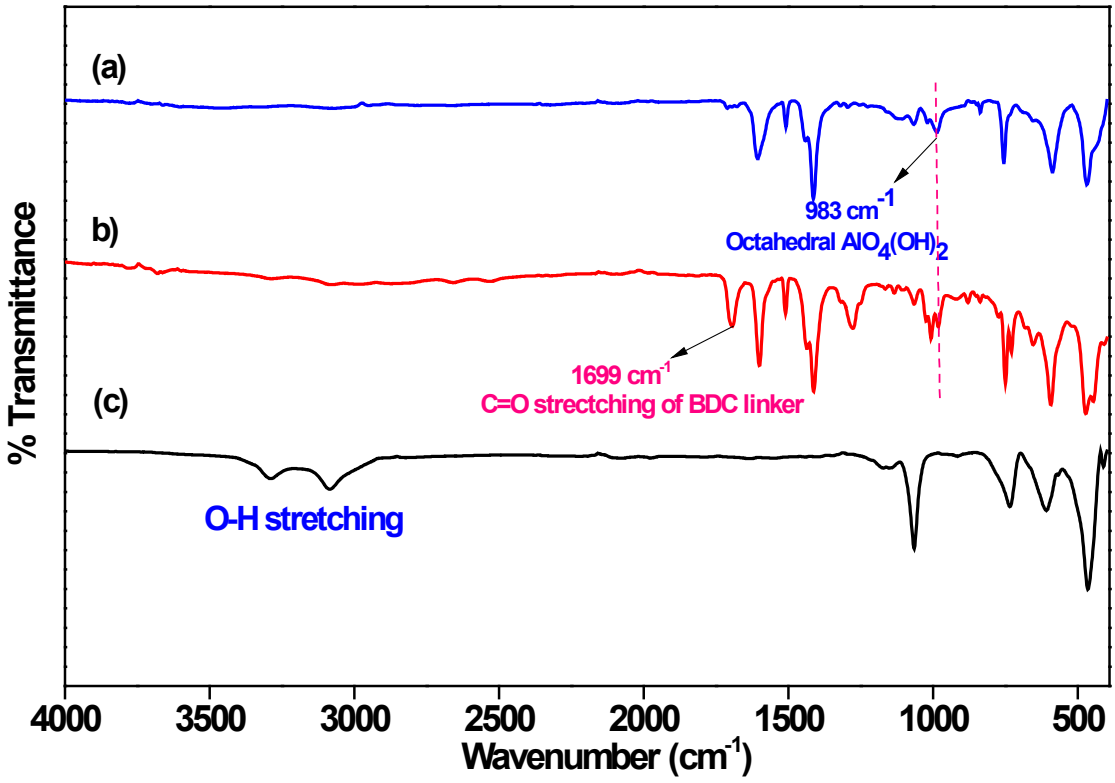

Figure 5: FTIR spectra of (a) MIL-53(Al)/biochar, (b) MIL-53(Al) and (c) activated bamboo biochar

3.1.4 Thermogravimetric Analysis (TGA)

Thermogravimetric analysis (TGA) was employed to evaluate the thermal stability and composition of the materials (Figure 6). For MIL-53(Al) (Figure 6b), an initial 6 wt% loss below 150 °C, corresponds to desorption of physisorbed and pore-confined water, followed by a major decomposition (32 wt%) between 450–600 °C (DTG maximum at 580 °C) corresponding to BDC linker degradation [49]. Activated biochar (Figure 6c) shows a single devolatilization step (≈ 21 wt% centered at 450 °C), attributed to pyrolytic cleavage of residual lignocellulosic fragments [50]. The composite (Figure 6a) shows a combined profile: (i) a minor 5 wt% loss below 150 °C (water), and (ii) a main degradation step of ≈ 28 wt% with DTG maximum at 550 °C. The slight shift to lower decomposition temperature compared with MIL-53(Al), suggests that intimate contact with the biochar matrix marginally catalyses MOF degradation, possibly due to catalytic oxygenated sites on the carbon surface. The framework stability up to ~350 °C, ensures resilience during typical adsorption–desorption regeneration cycles (< 250 °C).

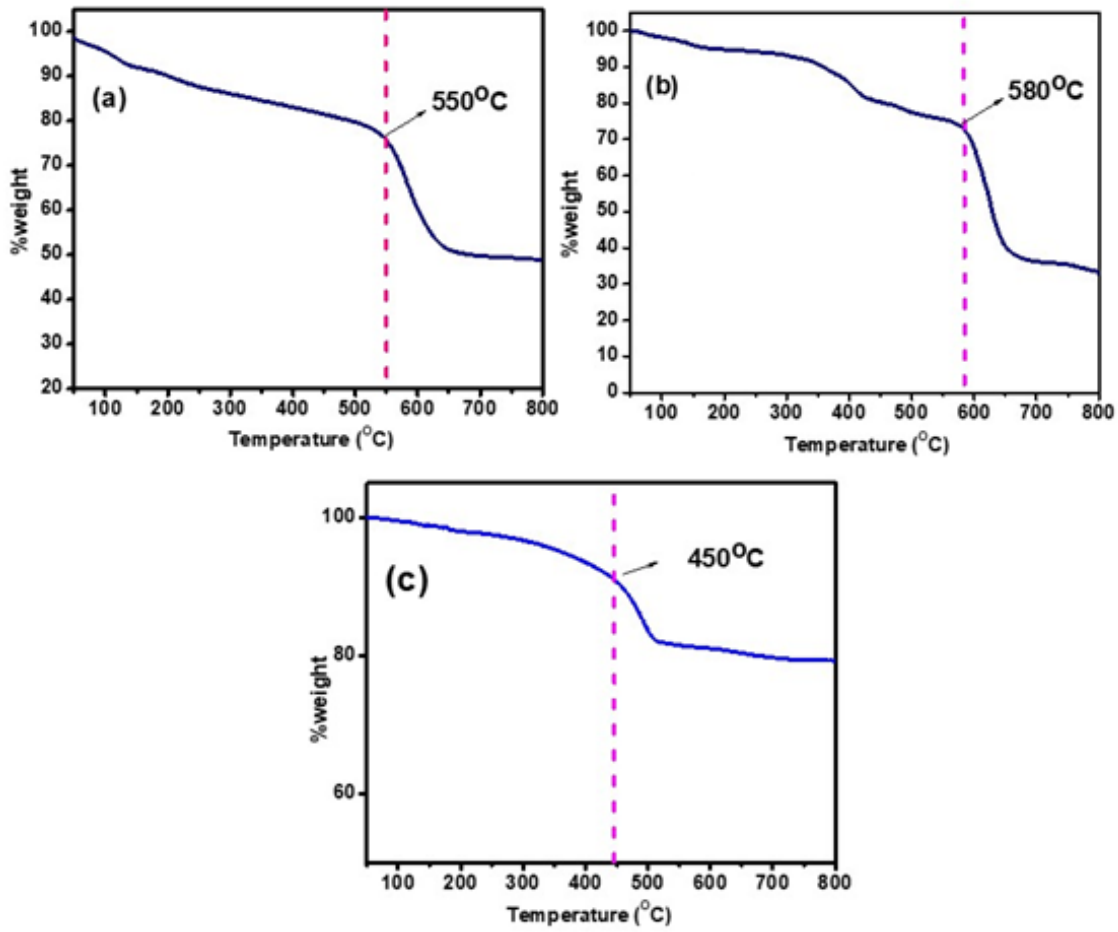

Figure 6: Thermogravimetric analysis (TGA) profile of (a) MIL 53(Al)/biochar, (b) MIL 53(Al) and (c) activated bamboo biochar.

3.2 Adsorption performance of MIL-53(Al) and MIL-53(Al)/Biochar Composite

3.2.1 Effect of Adsorbent Dosage and Initial NRFX Concentration on Adsorption Efficiency

Figure 7 shows the effect of adsorbent dosage on equilibrium capacity (q_e). Increasing the dose from 40 to 80 mg/L decreased the equilibrium capacity (q_e) for both materials: MIL-53(Al) decreased from 287 ± 6 to 190 ± 4 mg/g, while the composite declines from 300 ± 5 to 192 ± 3 mg/g at identical operating conditions. This inverse trend is common commonly observed in heterogeneous adsorption systems and is attributed to the saturation of available active sites at a fixed adsorbate concentration, as well as particle aggregation at higher loadings, which blocks surface sites and hinder mass transfer [51, 52]. Therefore, a dosage of 40 mg/L was selected for subsequent experiments, as it provided the highest adsorption capacity (300 mg/g) with ≥ 95% NRFX removal.

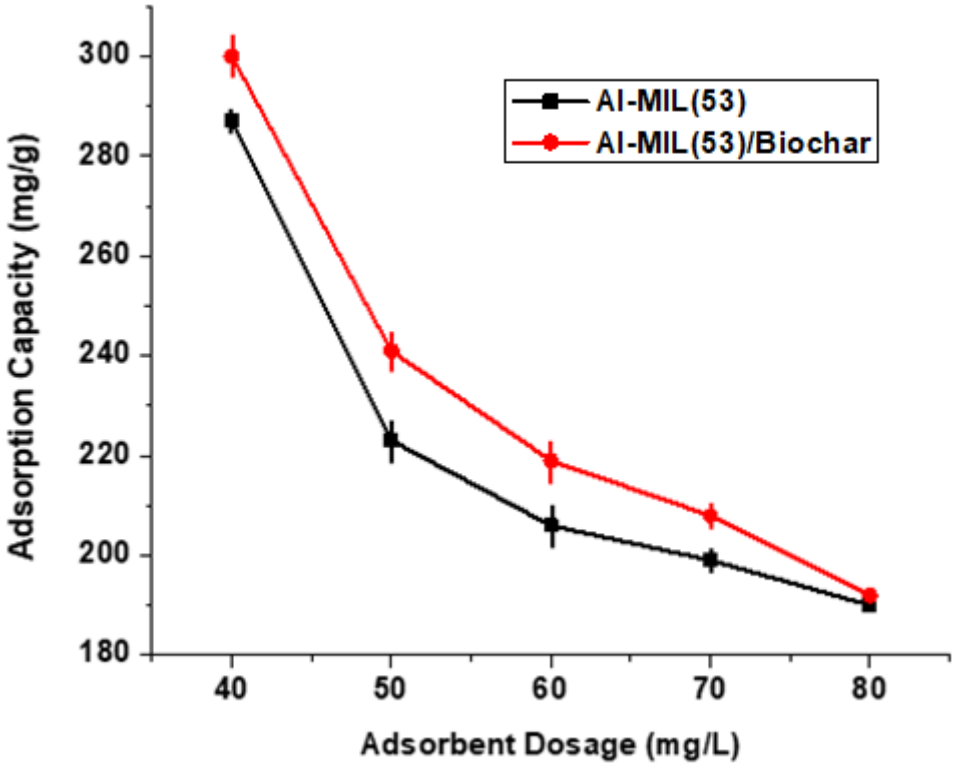

Figure 7: Effect of adsorbent dosage on NRFX adsorption by MIL-53(Al) and MIL-53(Al)/biochar composite at an initial NRFX concentration of 20 mg/L, temperature of 30 °C, and contact time of 120 min.

The effect of initial NRFX concentration (Figure 8) was evaluated over the range of 10–50 mg/L. For pristine MIL-53(Al), q_e increased from 242 ± 5 to 343 ± 7 mg/g, while for the MIL-53(Al)/BC

composite increases from 261 ± 6 to 357 ± 8 mg/g under identical conditions. The monotonic increase reflects the greater driving force for mass transfer at higher NRFX concentration enhancing solute–site collisions and accelerates surface coverage [53]. Across the entire range of NRFX concentration, the composite consistently delivered 6–8% higher capacity than that in pristine MIL-53(Al), reflecting the synergistic benefits of its larger surface area and higher mesopore fraction that facilitate faster intraparticle diffusion. Notably, the removal efficiency remains ≥ 90% even at the highest NRFX concentration (50 mg/L), confirming that MIL-53(Al)/BC not only provides a higher capacity per gram but also sustains superior performance under elevated contaminant loads an essential property for real-world wastewater treatment scenarios where antibiotic spikes can vary substantially.

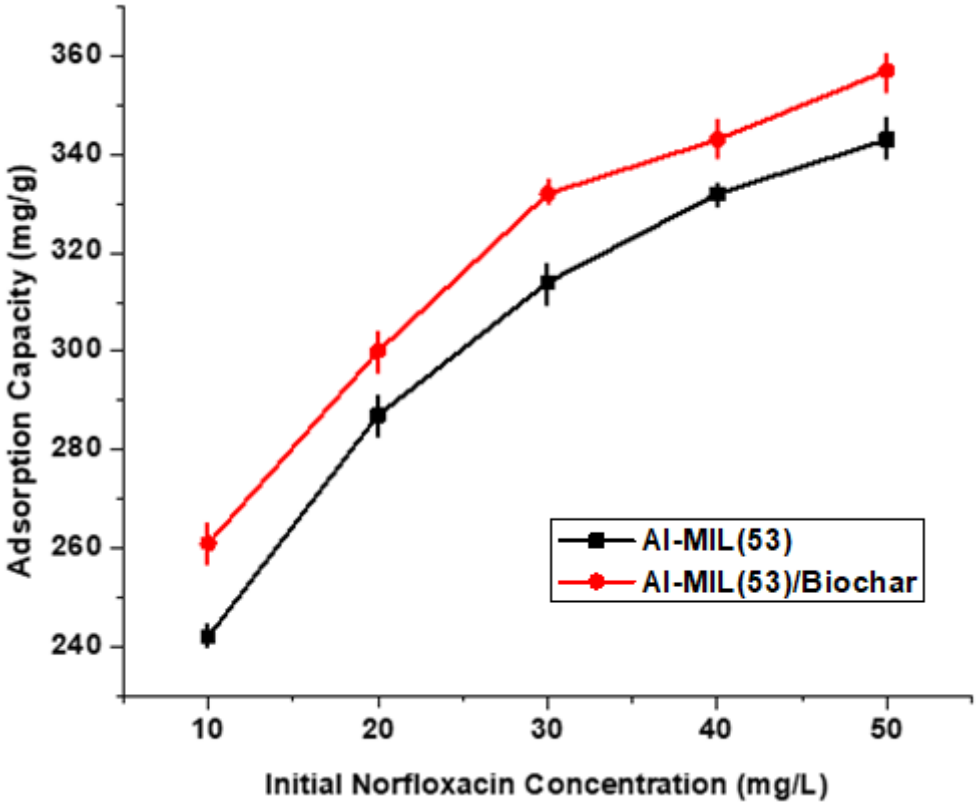

Figure 8: Effect of the initial NRFX concentration on NRFX adsorption by MIL-53(Al) and MIL-53(Al)/biochar composite at an adsorbent dosage of 40 mg/L, temperature of 30 °C, and contact time of 120 min.

3.2.2 Effect of Temperature on NRFX Adsorption Efficiency

Figure 9 examines the effect of temperature (30–70 °C) on the equilibrium capacity (q_e) of MIL-53(Al) and the MIL-53(Al)/biochar composite. For MIL-53(Al), q_e decreases from 288 ± 5 mg/g at

30 °C to 240 ± 4 mg/g at 70 °C (≈ 16% loss), while for MIL-53(Al)/BC it decreased from 300 ± 6 to 245 ± 5 mg/g (≈18% loss). This negative temperature coefficient confirms that NRFX adsorption is an exothermic process, consistent with previous fluoroquinolone studies reported elsewhere [54, 55]. The decline in capacity can be attributed to: (i) weakened hydrogen bonding and π–π interactions at elevated thermal energies [56], and (ii) reduced solution viscosity, which shortens solute–sorbent contact time [57]. Even at 70 °C the composite retained a high capacity (≥ 245 mg/g), outperforming many reported sorbents such as graphene oxide (≈ 200 mg/g), amine-functionalized magnetic bamboo-based activated carbon (≈ 293.2 mg/g) and KOH-activated biochar (≈ 180 mg/g) as well as MOF-based material e.g., ZIF-8 (≈ 210 mg/g), MIL-101 (≈ 222 mg/g) and MIL-53(FE) (≈ 240 mg/g) [58-60]. This combination of moderate thermal sensitivity and high residual capacity suggests that MIL-53(Al)/BC can perform effectively across typical wastewater temperatures (20–70 °C) and endure occasional thermal excursions during sunlight exposure or steam-assisted regeneration.

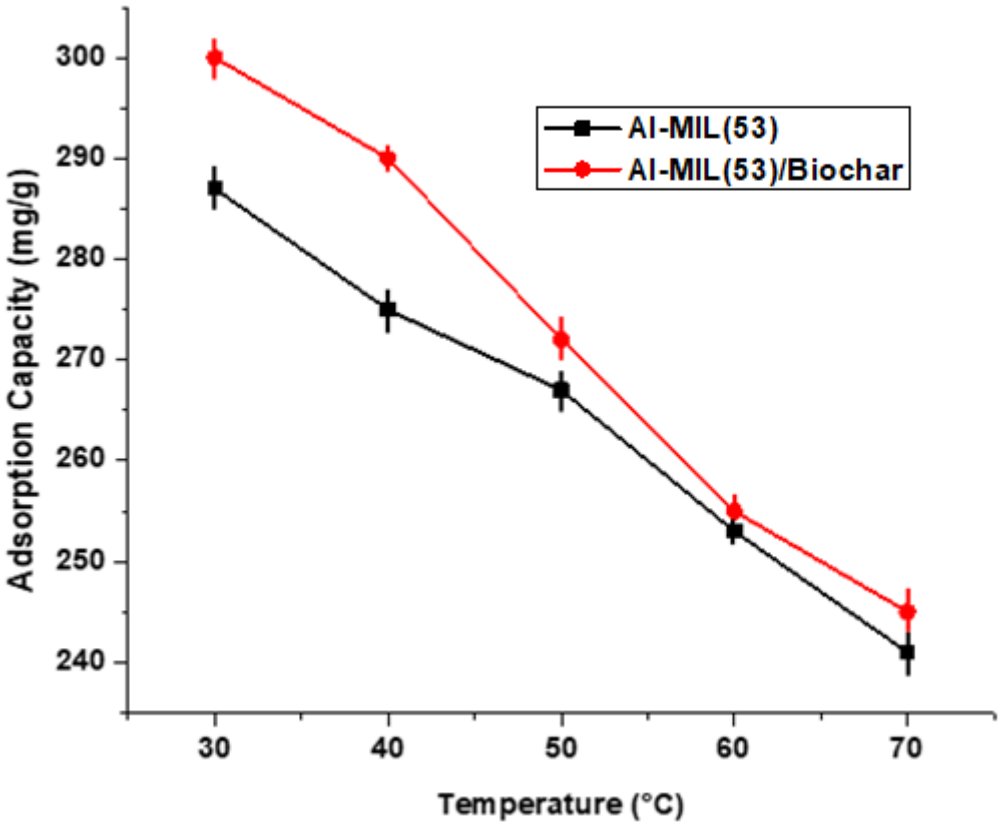

Figure 9: Effect of temperature on NRFX adsorption by MIL-53(Al) and MIL-53(Al)/biochar composite at an adsorbent dosage of 40 mg/L, NRFX concentration of 20 mg/L, and contact time of 120 min.

3.2.3 Effect of contact time on NRFX Adsorption Efficiency

Figure 10 shows the time-dependent uptake of NRFX on MIL-53(Al) and the MIL-53(Al)/biochar composite. Both adsorbents exhibit a biphasic pattern: an initial rapid phase within 15 min followed by a slower approach to equilibrium. The fast phase corresponds to external film diffusion and the abundance of vacant active sites, while the slower phase reflects intraparticle diffusion through MOF channels and the micro-mesoporous carbon matrix, governed by chemisorption such as hydrogen bonding, π–π stacking, and electrostatic attraction [61]. MIL-53(Al)/BC consistently achieved ~5% higher uptake than MIL-53(Al) across all time intervals at identical operating conditions and achieved 90% of equilibrium capacity within ~25 min, compared to typical carbon-based adsorbents e.g., KOH-activated biochar, graphene oxide and amine-functionalized magnetic bamboo-based activated and MOF sorbents such as ZIF-8, MIL-101 and MIL-53(FE) which often require > 120 min under comparable conditions [58-60]. The combination of rapid kinetics and high capacity underscores the practical suitability of MIL-53(Al)/BC for real-world antibiotic remediation.

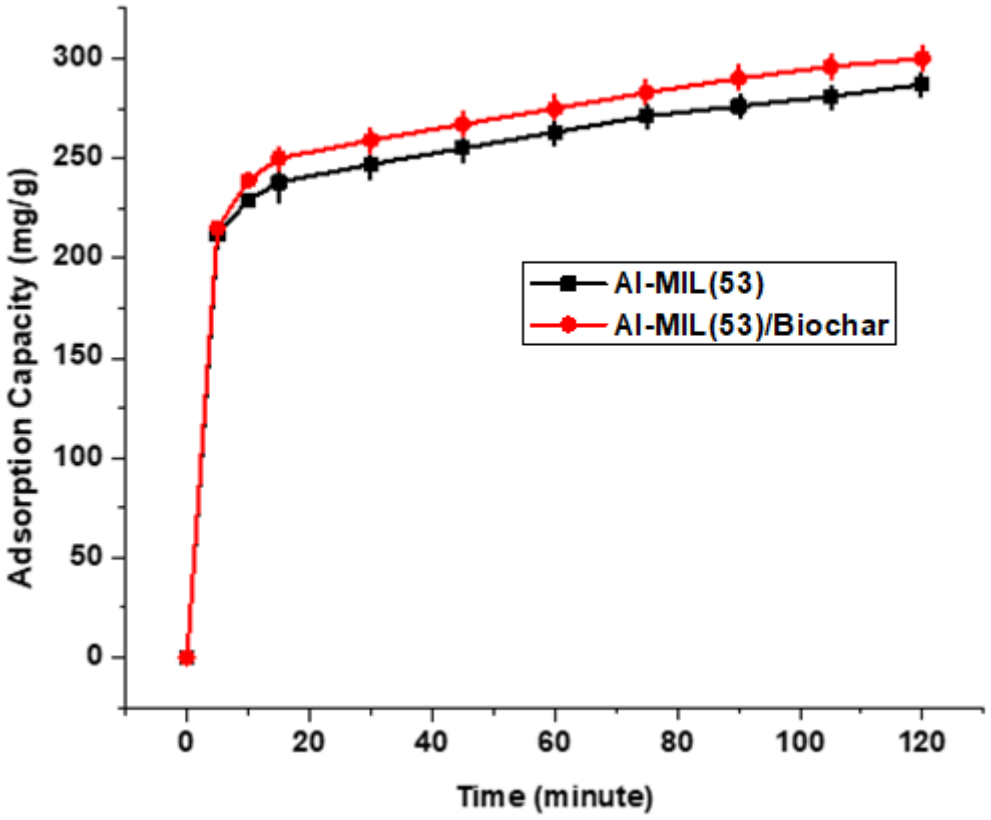

Figure 10: Effect of contact time on NRFX adsorption by MIL-53(Al) and MIL-53(Al)/biochar composite at an adsorbent dosage of 40 mg/L, initial NRFX concentration of 20 mg/L, and temperature of 30 °C.

3.3 Adsorption Mechanisms of NRFX

Figure 11 summarizes the adsorption mechanism of NRFX on MIL-53(Al)/biochar. First, hydrogen bonding: after adsorption FT-IR shows a red-shift of the NRFX carbonyl stretch from 1723 to 1711 cm^{-1} and an ~18% attenuation of the Al–OH band at 989 cm^{-1} (Figure 5), indicating hydrogen-bond formation between NRFX –COOH/–NH groups and –OH moieties on both MIL-53(Al) (Al–OH clusters) and activated biochar (phenolic and carboxylic groups). Second, electrostatic attraction: the composite surface carries a negative charge promoting Coulombic attraction between deprotonated carboxylate/phenolate sites and the protonated amine group of NRFX. Third, π- π interactions: the electron-rich quinolone ring of NRFX can interact with the conjugated π-electron systems of graphitic domains in biochar and the benzene rings of MIL-53(Al)'s terephthalate linkers (as described in sections 3.2.2 and 3.2.3). These π–π stacking and cation–π interactions enhance adsorption affinity, particularly in the presence of hydrophobic pockets within the composite. Finally, pore filling and van der Waals confinement: BET surface after NRFX uptake revealed a ~15% decrease in surface area (from 806 m^2/g for fresh MIL-53(Al)/biochar to 692 m^2/g for the spent MIL-53(Al)/biochar) and ~12% reduction in micropore volume (from 0.5 cm^2/g to 0.3 m^2/g), suggesting that NRFX molecules partially occupy MIL-53(Al) channels and mesoporous biochar network, where van der Waals forces stabilize the adsorbed species. This multi-modal adsorption mechanism combining hydrogen bonding, electrostatic attraction, π–π stacking, and physical confinement has also been reported for other MOF–biochar hybrids such as montmorillonite–biochar composites and Fe–BTC/polydopamine microspheres [62, 63].

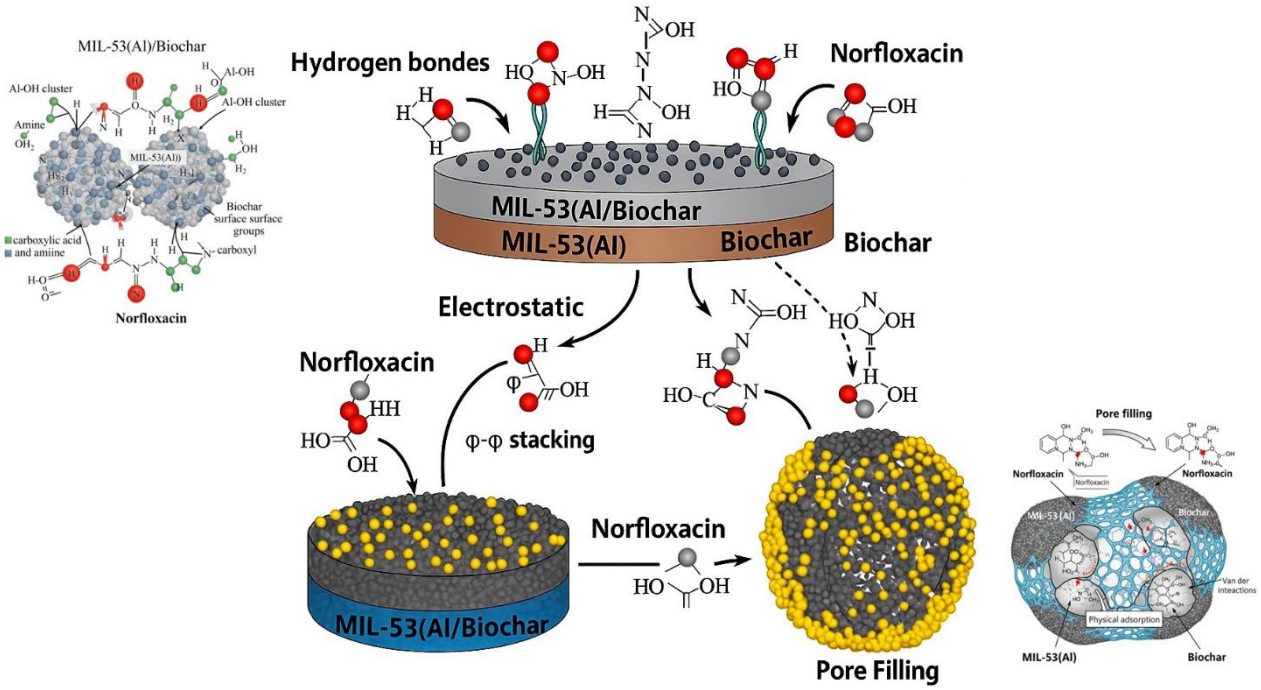

Figure 11: The proposed adsorption mechanism of NRFX on the MIL-53(Al)/biochar composite

4. Conclusion

This study demonstrates the successful synthesis a novel MIL-53(Al)/biochar composite via an in situ hydrothermal approach, integrating the flexibility of MIL-53(Al)'s "wine-rack" framework of MIL-53(Al) with the oxygen-functionalized, mesoporous carbon matrix of bamboo-derived biochar. The resulting hybrid exhibited a high specific surface area (806 m^2/g), increased pore volume, and a hierarchical micro–mesoporous network, enabling enhanced mass transfer and abundant active sites for NRFX adsorption. Under optimal conditions (20 mg/L NRFX, 40 mg/L adsorbent, 30 °C, 120 min), MIL-53(Al)/BC achieved an exceptional adsorption capacity of 357 mg/g, significantly outperforming most MOF and carbon-based adsorbents reported in the literature, which typically exhibit capacities below 250 mg/g. The superior performance was attributed to a synergistic multi-modal adsorption mechanism involving hydrogen bonding, electrostatic attraction, π–π interactions, and pore-filling effects, as confirmed by FT-IR and BET analyses. Furthermore, the composite also demonstrated rapid uptake kinetics, reaching 90% of equilibrium capacity within ~25 min, and maintained high residual capacity across a wide temperature range (20–70 °C), confirming its potential for practical wastewater treatment.

To advance practical application, future research should prioritize: (i) scaling up synthesis under industrially feasible conditions, (ii) evaluating long-term stability and regeneration over multiple adsorption–desorption cycles, and (iii) validating performance in real wastewater matrices

with diverse co-contaminants. In addition, life-cycle aspects including solvent consumption, energy demand, and the environmental footprint of regeneration must be critically assessed to ensure that the promising laboratory-scale performance of MIL-53(Al)/biochar can be translated into sustainable and industrially viable water treatment solutions.

References

1. Chaturvedi, P., Shukla, P., Giri, B. S., Chowdhary, P., Chandra, R., Gupta, P., & Pandey, A. (**2021**). Prevalence and hazardous impact of pharmaceutical and personal care products and antibiotics in environment: A review on emerging contaminants. *Environmental Research*, 194, 110664.
2. Kumar, M., Sridharan, S., Sawarkar, A. D., Shakeel, A., Anerao, P., Mannina, G., Sharma, P., & Pandey, A. (**2023**). Current research trends on emerging contaminants pharmaceutical and personal care products (PPCPs): a comprehensive review. *Science of the total environment*, 859, 160031.
3. Narayanan, M., El-sheekh, M., Ma, Y., Pugazhendhi, A., Natarajan, D., Kandasamy, G., Raja, R., Saravana Kumar, R., Kumarasamy, S., Sathiyan, G., Geetha, R., Paulraj, B., Liu, G., & Kandasamy, S. (**2022**). Current status of microbes involved in the degradation of pharmaceutical and personal care products (PPCPs) pollutants in the aquatic ecosystem. *Environmental Pollution*, 300, 118922.
4. Sim, W., Kim, H., Choi, S., Kwon, J., & Oh, J. (**2013**). Evaluation of pharmaceuticals and personal care products with emphasis on anthelmintics in human sanitary waste, sewage, hospital wastewater, livestock wastewater and receiving water. *Journal of Hazardous Materials*, 248-249, 219-227.
5. Hawash, H. B., Moneer, A. A., Galhoum, A. A., Elgarahy, A. M., Mohamed, W. A., Samy, M., El-Seedi, H. R., Gaballah, M. S., Mubarak, M. F., & Attia, N. F. (**2023**). Occurrence and spatial distribution of pharmaceuticals and personal care products (PPCPs) in the aquatic environment, their characteristics, and adopted legislations. *Journal of Water Process Engineering*, 52, 103490.
6. Mojtabavi, S., Rezayaraghi, F., Shahverdi, M., Golroudbari, H. T., Moshiri, F., & Faramarzi, M. A. (**2023**). Bioremoval and biodetoxification of ciprofloxacin from hospital wastewater effluent by the efficient and recyclable laccase@hercynite magnetic nanoparticles. *Journal of Environmental Chemical Engineering*, 11(6), 111599.
7. Gerbersdorf, S. U., Cimatoribus, C., Class, H., Engesser, K.-H., Helbich, S., Hollert, H., Lange, C., Kranert, M., Metzger, J., & Nowak, W. (**2015**). Anthropogenic Trace Compounds (ATCs) in aquatic habitats—Research needs on sources, fate, detection and toxicity to ensure timely elimination strategies and risk management. *Environment International,* 79, 85-105.
8. Rathi, B. S., Kumar, P. S., & Vo, D.-V. N. (**2021**). Critical review on hazardous pollutants in water environment: Occurrence, monitoring, fate, removal technologies and risk assessment. *Science of the total environment*, 797, 149134.

9. Ahmad, I., Malak, H. A., & Abulreesh, H. H. (**2021**). Environmental antimicrobial resistance and its drivers: a potential threat to public health. *Journal of Global Antimicrobial Resistance*, 27, 101-111.
10. Ferri, M., Ranucci, E., Romagnoli, P., & Giaccone, V. (**2017**). Antimicrobial resistance: A global emerging threat to public health systems. *Critical reviews in food science and nutrition*, 57(13), 2857-2876.
11. Serwecińska, L. (**2020**). Antimicrobials and antibiotic-resistant bacteria: a risk to the environment and to public health. *Water*, 12(12), 3313.
12. Wei, F., Liu, H., Ren, Q., Yang, L., Qin, L., Chen, H., Ma, Y., Liang, Z., & Wang, S. (**2023**). Preparation of Zr-MOF for the removal of Norfloxacin from an aqueous Solution. *Inorganic Chemistry Communications*, 153, 110819.
13. Zhang, G., Xue, Y., Wang, Q., Wang, P., Yao, H., Zhang, W., Zhao, J., & Li, Y. (2019). Photocatalytic oxidation of norfloxacin by $Zn_{0.9}Fe_{0.1}S$ supported on Ni-foam under visible light irradiation. *Chemosphere*, 230, 406-415.
14. Zhuang, Y., & Luan, J. (**2020**). Improved photocatalytic property of peony-like InOOH for degrading norfloxacin. *Chemical Engineering Journal*, 382, 122770.
15. Haque, M., & Muneer, M. (**2007**). Photodegradation of norfloxacin in aqueous suspensions of titanium dioxide. *Journal of Hazardous materials*, 145(1-2), 51-57.
16. Dodd, M. C., Kohler, H.-P. E., & Von Gunten, U. (**2009**). Oxidation of antibacterial compounds by ozone and hydroxyl radical: elimination of biological activity during aqueous ozonation processes. *Environmental Science & Technology*, 43(7), 2498-2504.
17. Tang, L., Wang, J., Zeng, G., Liu, Y., Deng, Y., Zhou, Y., Tang, J., Wang, J., & Guo, Z. (**2016**). Enhanced photocatalytic degradation of norfloxacin in aqueous Bi_2WO_6 dispersions containing nonionic surfactant under visible light irradiation. *Journal of Hazardous materials*, 306, 295-304.
18. Li, L., Zhao, J., Sun, Y., Yu, F., & Ma, J. (**2019**). Ionically cross-linked sodium alginate/κ-carrageenan double-network gel beads with low-swelling, enhanced mechanical properties, and excellent adsorption performance. *Chemical Engineering Journal*, 372, 1091-1103.
19. Shi, T., Peng, J., Chen, J., Sun, C., & He, H. (**2017**). Heterogeneous photo-fenton degradation of norfloxacin with Fe_3O_4-multiwalled carbon nanotubes in aqueous solution. *Catalysis Letters*, 147, 1598-1607.
20. Akhtar, M. S., Ali, S., & Zaman, W. (**2024**). Innovative adsorbents for pollutant removal: Exploring the latest research and applications. *Molecules*, 29(18), 4317.

21. de Jesús Ruíz-Baltazar, Á. (**2024**). Advancements in nanoparticle-modified zeolites for sustainable water treatment: An interdisciplinary review. *Science of the total environment*, 174373.
22. Kumar, M., Chowdhury, S., & Randhawa, J. K. (**2024**). Emerging trends in membrane-based wastewater treatment: electrospun nanofibers and reticular porous adsorbents as key components. Environmental Science: *Water Research & Technology*, 10(1), 29-84.
23. Liaquat, I., Munir, R., Abbasi, N. A., Sadia, B., Muneer, A., Younas, F., Sardar, M. F., Zahid, M., & Noreen, S. (**2024**). Exploring zeolite-based composites in adsorption and photocatalysis for toxic wastewater treatment: Preparation, mechanisms, and future perspectives. *Environmental Pollution*, 123922.
24. Satyam, S., & Patra, S. (2024). Innovations and challenges in adsorption-based wastewater remediation: A comprehensive review. *Heliyon*, *10*(9), e29573.
25. He, Y., Wang, Z., Wang, H., Wang, Z., Zeng, G., Xu, P., Huang, D., Chen, M., Song, B., & Qin, H. (**2021**). Metal-organic framework-derived nanomaterials in environment related fields: Fundamentals, properties and applications. *Coordination Chemistry Reviews*, 429, 213618.
26. Mane, P. V., Rego, R. M., Yap, P. L., Losic, D., & Kurkuri, M. D. (**2024**). Unveiling cutting-edge advances in high surface area porous materials for the efficient removal of toxic metal ions from water. *Progress in Materials Science*, 101314.
27. Rasheed, T. (**2023**). Water stable MOFs as emerging class of porous materials for potential environmental applications. *Chemosphere*, 313, 137607.
28. Millange, F., & Walton, R. I. (**2018**). MIL-53 and its isoreticular analogues: a review of the chemistry and structure of a prototypical flexible metal-organic framework. *Israel Journal of Chemistry,* 58(9-10), 1019-1035.
29. Tomar, S., & Singh, V. (**2021**). Review on synthesis and application of MIL-53. *Materials Today: Proceedings,* 43, 3291-3296.
30. Zou, M., Tian, W., Chu, M., Chen, Z. (**2024**). Effective adsorption of norfloxacin from water on magnetic biochar composite derived from cellulase hydrolysis apple branch: Synthesis optimization, performance assessment and mechanism insight. *Process Safety and Environmental Protection,* 185, 435–444.
31. Yang, Z., Yuan, D., Liu, S., Wang, J., Chen, Y., & Zhang, H. (**2022**). Biochar-supported magnetic MIL-53(Fe) derivatives as an efficient catalyst for peroxydisulfate activation towards antibiotics degradation. *Applied Catalysis B: Environmental,* 317, 121768.

32. Ohale, P. E., Igwegbe, C. A., Iwuozor, K. O., & Okoro, B. C. (**2023**). A review of the adsorption method for norfloxacin reduction from aqueous media. *MethodsX,* 10, 102180.
33. Chakhtouna, H., Benzeid, H., Zari, N., Qaiss, A. E. K., & Bouhfid, R. (**2023**). Microwave-assisted synthesis of MIL-53(Fe)/biochar composite from date palm for ciprofloxacin and ofloxacin antibiotics removal. *Separation and Purification Technology*, 308, 122850.
34. Fernández-Andrade, N., Cevallos-Mendoza, J. E., Cedeño-Muñoz, J. S., Montenegro, M. C. B. S., & Rodríguez-Díaz, J. M. (**2024**). Development of hybrid MIL-53(Al)@CBS for ternary adsorption of tetracyclines antibiotics in water: Physical interpretation of the adsorption mechanism. *Bioresource Technology*, 396, 130453.
35. Tong, J., Chen, L., Cao, J., Yang, Z., Xiong, W., Jia, M., Xiang, Y., & Peng, H. (**2022**). Biochar supported magnetic MIL-53-Fe derivatives as an efficient catalyst for peroxydisulfate activation towards antibiotics degradation. *Separation and Purification Technology*, *294*, 121064.
36. Ge, Q., Li, P., Liu, M., Xiao, G., Xiao, Z., Mao, J., & Gai, X. (**2023**). Removal of methylene blue by porous biochar obtained by KOH activation from bamboo biochar. *Bioresources and Bioprocessing,* 10(1), 1-14.
37. Meshram, A. A., & Sontakke, S. M. (2021). Synthesis of highly stable nanoscale MIL-53 MOF and its application for the treatment of complex mixed dye solutions and real-time dye industry effluent. *Separation and Purification Technology,* 274, 119073.
38. Li, C., Xiong, Z., Zhang, J., & Wu, C. (2015). The strengthening role of the amino group in Metal–Organic Framework MIL-53 (AL) for methylene blue and malachite green dye adsorption. *Journal of Chemical & Engineering Data,* 60(11), 3414–3422.
39. Chen, Q., He, Q., Lv, M., Xu, Y., Yang, H., Liu, X., & Wei, F. (2014). Selective adsorption of cationic dyes by UiO-66-NH2. *Applied Surface Science,* 327, 77–85.
40. Ahadi, N., Askari, S., Fouladitajar, A., & Akbari, I. (2022). Facile synthesis of hierarchically structured MIL-53(Al) with superior properties using an environmentally-friendly ultrasonic method for separating lead ions from aqueous solutions. *Scientific Reports,* 12(1), 1-17.
41. Silvester, L., Naim, A., Fateeva, A., Postole, G., Auroux, A., Massin, L., Gelin, P., & Bois, L. (**2020**). Fine tuning of the physico-chemical properties of a MIL-53(Al) type - Mesoporous alumina composite using a facile sacrificial-template synthesis approach. *Microporous and Mesoporous Materials,* 306, 110443.

42. Yan, J., Jiang, S., Ji, S., Shi, D. & Cheng, H. (**2015**) Metal-organic framework MIL-53(Al): Synthesis, catalytic performance for the Friedel-Crafts acylation, and reaction mechanism. *Sci. China Chem.* 58, 1544–1552.
43. Li, J., Wu, Y. N., Li, Z., Zhu, M. & Li, F. (**2014**) Characteristics of arsenate removal from water by metal-organic frameworks (MOFs). *Water Sci. Technol.* 70, 1391–1397.
44. Kim, Y., Park, Y., Han, S., Park, W., Kim, M., Kim, K., Joo, J., Hahn, S. K., & Kwon, W. (**2022**). Radiative and Non-Radiative Decay Pathways in Carbon Nanodots toward Bioimaging and Photodynamic Therapy. *Nanomaterials*, 12(1), 70.
45. Ge, J., Liu, L., Qiu, L., Jiang, X. & Shen, Y. (**2016**) Facile synthesis of amine-functionalized MIL-53(Al) by ultrasound microwave method and application for CO2 capture. *J. Porous Mater.* 23, 857–865.
46. Serre, C., Millange, F., Thouvenot, C., Noguès, M., Marsolier, G., Louër, D., & Férey, G. (**2002**). Very large breathing effect in the first nanoporous chromium(III) metal–organic framework MIL-53. *Chemistry of Materials*, 14, 1805-1812.
47. Abdollahi, M., & Emam, H. (**2021**). Current progress in degradation and removal methods of polybrominated diphenyl ethers from water and soil: A review. *Journal of Hazardous Materials*, 403, 123674.
48. Guo, X., Li, Y., & Zhao, B. (**2023**). High-efficiency ternary sequential solution deposition structure organic solar cells with two polymer donors. *Chemical Engineering Journal*, 452, 139462.
49. Sánchez-Sánchez, M., Getachew, N., Díaz, K., Díaz-García, M., Chebude, Y., & Díaz, I. (**2014**). Synthesis of metal–organic frameworks in water at room temperature: salts as linker sources. *Green Chemistry*, 17(3), 1500–1509.
50. Cao, X., Zhong, L., Peng, X., Sun, S., Li, S., Liu, S., & Sun, R. (**2014**). Comparative study of the pyrolysis of lignocellulose and its major components: Characterization and overall distribution of their biochars and volatiles. *Bioresource Technology*, 155, 21-27.
51. Wan, Y., Liu, X., Liu, P., Zhao, L., & Zou, W. (**2018**). Optimization adsorption of norfloxacin onto polydopamine microspheres from aqueous solution: Kinetic, equilibrium and adsorption mechanism studies. *Science of The Total Environment*, 639, 428-437.
52. Foo, K. Y., & Hameed, B. H. (**2010**). Insights into the modeling of adsorption isotherm systems. *Chemical Engineering Journal*, 156, 2-10.

53. Ohale, P. E., Igwegbe, C. A., Iwuozor, K. O., Emenike, E. C., Obi, C. C., & Białowiec, A. (**2022**). A review of the adsorption method for norfloxacin reduction from aqueous media. *MethodsX*, 10, 102180.
54. Chen, J., Zhang, J., Wang, W., Ma, X., Guo, Y., Sun, F., & Wang, Y. (**2020**). Comparison of adsorption characteristics of acid-base modified fly ash to norfloxacin. *Spectroscopy Letters*, 53(6), 416–429.
55. Moreira, V.R., Lebron, Y.A.R., da Silva, M.M. (**2020**), Graphene oxide in the remediation of norfloxacin from aqueous matrix: simultaneous adsorption and degradation process. *Environ Sci Pollut Res* 27, 34513–34528.
56. Fan, Y.-H.; Zhang, S.-W.; Qin, S.-B.; Li, X.-S.; Qi, S.-H. (**2018**). An enhanced adsorption of organic dyes onto NH_2-functionalization titanium-based metal–organic frameworks and the mechanism investigation. *Microporous and Mesoporous Materials* 263. 120–127.
57. Lin, K., Wang, K., Chen, Y., & Ma, J. (**2015**). Temperature-dependent adsorption kinetics of norfloxacin on ordered mesoporous carbon: Role of solution viscosity and surface interaction energy. *Journal of Colloid and Interface Science*, 453, 126-134.
58. Khan, M. S.; Li, Y.; Li, D.; Qiu, J.; Xu, X.; Yang, H. Y. (**2023**). A review of metal–organic framework (MOF) materials as an effective photocatalyst for degradation of organic pollutants. *Nanoscale Advances* 5 (23). 6318–6348.
59. Hu, X., Lu, X., Luo, F., & Chen, Y. (**2017**). Graphene oxide as a highly efficient adsorbent for removal of fluoroquinolone antibiotics from water. *Journal of Hazardous Materials,* 335, 457-466.
60. Zeng, Z., Zhang, J., Qu, X., Zheng, D., Liang, H., & Yang, G. (**2018**). Adsorption of norfloxacin on ZIF-8: Kinetics, isotherms and mechanisms. *Chemical Engineering Journal*, 359, 26-34.
61. Chen, S., Qin, C., Wang, T., Chen, F., Li, X., Hou, H., & Zhou, M. (**2019**). Study on the adsorption of dyestuffs with different properties by sludge-rice husk biochar: Adsorption capacity, isotherm, kinetic, thermodynamics and mechanism. *Journal of Molecular Liquids*, 285, 62-74.
62. Darweesh, T. M., & Ahmed, M. J. (**2017**). Adsorption of ciprofloxacin and norfloxacin from aqueous solution onto granular activated carbon in fixed bed columns. *Ecotoxicology and Environmental Safety*, 138, 139-145.
63. Peng, H., Pan, B., Wu, M., Liu, Y., Zhang, D., & Xing, B. (**2012**). Adsorption of ofloxacin and norfloxacin on carbon nanotubes: Hydrophobicity- and structure-controlled process. *Journal of Hazardous Materials,* 233-234, 89-96.